# In-Fiber Acousto-Optic Interaction Based on Flexural Acoustic Waves and Its Application to Fiber Modulators

Miguel Ángel Bello Jiménez,

Gustavo Ramírez-Meléndez,

Erika Hernández-Escobar, Andrés Camarillo-Avilés,

Rosa López-Estopier, Olivier Pottiez,

Cristian Cuadrado-Laborde, Antonio Díez,

José L. Cruz and Miguel V. Andrés

Additional information is available at the end of the chapter

## Abstract

The design and implementation of in-fiber acousto-optic (AO) devices based on acoustic flexural waves are presented. The AO interaction is demonstrated to be an efficient mechanism for the development of AO tunable filters and modulators. The implementation of tapered optical fibers is proposed to shape the spectral response of in-fiber AO devices. Experimental results demonstrate that the geometry of the tapered fiber can be regarded as an extra degree of freedom for the design of AO tunable attenuation filters (AOTAFs). In addition, with the objective of expanding the application of AOTAFs to operate as an amplitude modulator, acoustic reflection was intentionally induced. Hence, a standing acoustic wave is generated which produces an amplitude modulation at twice the acoustic frequency. As a particular case, an in-fiber AO modulator composed of a double-ended tapered fiber was reported. The fiber taper was prepared using a standard fusion and pulling technique, and it was tapered down to a fiber diameter of 70 μm. The device exhibits an amplitude modulation at 2.313 MHz, which is two times the acoustic frequency used (1.1565 MHz); a maximum modulation depth of 60%, 1.3 dB of insertion loss, and 40 nm of modulation bandwidth were obtained. These results are within the best results reported in the framework of in-fiber AO modulators.

**Keywords:** acousto-optic interaction, acousto-optic filter, acousto-optic modulator

## 1. Introduction

The acousto-optic (AO) effect based on flexural acoustic waves in optical fibers has received a great deal of attention for the development of many practical AO devices such as frequency shifters, attenuators, and tunable filters [1–3]. In recent years, novel AO devices have been proposed and developed to explore applications of in-fiber AO interaction in a different way, for example, by implementing standing flexural acoustic waves [4, 5] or by the use acoustic waves in short packets [6]. All these approaches offer the advantages of being dynamic devices with tunable amplitude and spectral responses. Its operation principle relies on the intermodal coupling induced by flexural acoustic waves along the fiber. The propagation of the acoustic field produces a periodic perturbation of the refractive index that leads to an intermodal resonant coupling between the fundamental core mode and some asymmetric cladding modes of the fiber [1–3]. This AO effect produces a similar response to that obtained with a conventional long-period grating (LPG), but in this case, the transmission response can be controlled dynamically by the amplitude and frequency of the acoustic wave.

In the framework of all-fiber modulators that exploit the dynamic properties of AO interaction, several alternatives have been proposed and demonstrated [4, 6–15]. Among them, we have proposed a modulation technique based on the intermodal coupling induced by standing flexural acoustic waves in a standard optical fiber [4, 15]. This novel type of modulator provides a stable amplitude modulation that can be used to realize mode-locking operation in a fiber laser system [4, 15]. However, its major shortcoming is the reduced modulation bandwidth (~1.5 nm), which could be a detrimental factor for systems that require broader optical bandwidths. In this chapter we report an improved version of the AO modulator by implementing tapered optical fibers as the mechanism to optimize the spectral response. The results demonstrate that the geometry of the tapered fiber can be regarded as an extra degree of freedom to the design of AO tunable modulators. For the particular case of 70 μm fiber modulator, high modulation depth of 60%, low insertion loss of 1.3 dB, and 40 nm of modulation bandwidth are achieved. If we compare this result with conventional non-tapered modulators [4, 15], we can appreciate the improvement achieved with the present scheme.

In Section 2, we start with the numerical modeling of acoustically induced LPG formed in a tapered structure. Then, in Section 3, we describe the experimental results and compare with numerical simulations to obtain insight into the effect of including tapered optical fiber in the AO device. Finally, our conclusions are summarized in Section 4.

## 2. Numerical modeling of the acousto-optic interaction in optical fibers

From the mechanical point of view, optical fibers are homogeneous cylinders immersed in air that have the ability to guide acoustic waves. These acoustic waves, depending on the displacement of their particles, are classified as flexural, longitudinal, or torsional waves. For the case of the flexural waves, a vibration is generated in one of the transverse directions of the fiber, which produces an asymmetric perturbation of the refractive index. In this section, the numerical technique to simulate the spectral response of the acoustically induced LPG is

presented. Following the theory developed by Birks et al. in Ref. [3], the transmission matrix to numerically simulate the intermodal coupling between the core and cladding forward-propagating modes is reported.

The perturbation of the refractive index, $\Delta n(x,y)$, is described in terms of the acoustic wave as follows:

$$\Delta n(x, y) = \Delta n_0 \, \sin\,(\Omega t - Kz), \tag{1}$$

$$\Delta n_0 = n_0(1 - \chi)\, K^2 \, u_0 \, y, \tag{2}$$

where $x$, $y$, and $z$ are the Cartesian coordinates. $z$ represents the direction of propagation along the fiber for both the light and the acoustic wave, $K$ is the acoustic wave number, $\Omega$ is the acoustic wave angular frequency, and $\Delta n_0$ is the perturbation amplitude (defined in Eq. (2)) with $n$ being the refractive index of the fiber glass, $\chi$ is the photoelastic coefficient ($\chi = 0.22$ for silica), and $u_0$ is the amplitude of vibration of the flexural acoustic wave, which is assumed to vibrate in the direction of the $y$-axis. The coupling coefficient ($\kappa$) between the fundamental mode and a cladding mode is evaluated with the expression

$$\kappa = \frac{\omega}{2c} \iint\limits_{A} \Delta n_0 E_{01}^* E_{lm} \; dx \, dy \tag{3}$$

where $\omega$ is the optical angular frequency, $c$ is the speed of light, and $E_{lm}$ is the normalized amplitude of the electric field of a fiber mode, being $l = 0$ and $m = 1$ the fundamental mode where * denotes the complex conjugate.

The fact that the perturbation has an explicit dependence on the transverse coordinate $y$ implies a sinusoidal dependence with the azimuthal coordinate $\phi$, $y = r \sin\phi$, which leads to an antisymmetric distribution of the perturbation in the cross section $A$ of the fiber. Because the field distribution of the fundamental mode ($LP_{01}$) is symmetrical, to prevent the coupling coefficient from being null, the energy coupling is restricted to the cladding modes with asymmetric distribution. The modes that feature this asymmetric distribution feature are the $LP_{1m}$ modes. Thus, there will be an intermodal coupling between the mode $LP_{01}$ and the asymmetric modes of the family $LP_{1m}$. The total optical field is a superposition of two modes, which correspond to the core and cladding forward-propagating modes with local amplitudes $A(z)$ and $B(z)$, respectively. These amplitudes satisfy the following pair of coupled-mode equations:

$$\frac{dA(z)}{dz} = -j \, \kappa \, B(z) \, e^{j\Omega t} \, e^{2j\delta z} \tag{4}$$

$$\frac{dB(z)}{dz} = -j \, \kappa \, A(z) \, e^{-j\Omega t} \, e^{-2j\delta z} \tag{5}$$

where $j = (-1)^{1/2}$; $\delta = (1/2)(\beta_{01}: \beta_{lm}): (\pi/\Lambda)$ is the phase mismatch parameter; $\beta_{01}$ and $\beta_{lm}$ are the propagation constants for the fundamental core mode and a high-order cladding mode, respectively; and $\Lambda$ is the wavelength of the acoustic wave ($K = 2\pi/\Lambda$). In the regime of low frequencies, $\Lambda$ can be expressed as

$$\Lambda = \sqrt{\frac{\pi a c_{ext}}{f}}, \tag{6}$$

where $a$ is the radius of the fiber, $c_{ext}$ is the extensional velocity (5760 m/s for silica), and $f$ is the acoustic frequency.

The mode amplitudes, and hence the electric fields, can be readily solved from Eqs. (4) and (5) in terms of a matrix $F$ [16]:

$$\begin{bmatrix} A(z)e^{-j\beta_{01}z} \\ B(z)e^{-j\beta_{lm}z} \end{bmatrix} = F \begin{bmatrix} A(0) \\ B(0) \end{bmatrix}, \tag{7}$$

$$F = \begin{bmatrix} \left( \cos(\gamma z) - j\dfrac{\delta}{\gamma} \sin(\gamma z) \right) e^{-j\left(\overline{\beta}+\frac{\pi}{\Lambda}\right)z} & \left( -\dfrac{\kappa}{\gamma} e^{jKz} \sin(\gamma z) \right) e^{-j\left(\overline{\beta}+\frac{\pi}{\Lambda}\right)z} \\ \left( \dfrac{\kappa}{\gamma} e^{-jKz} \sin(\gamma z) \right) e^{-j\left(\overline{\beta}-\frac{\pi}{\Lambda}\right)z} & \left( \cos(\gamma z) + j\dfrac{\delta}{\gamma} \sin(\gamma z) \right) e^{-j\left(\overline{\beta}-\frac{\pi}{\Lambda}\right)z} \end{bmatrix}, \tag{8}$$

where $\gamma = \left( \delta^2 + \kappa^2 \right)^{1/2}$ and $\overline{\beta} = \frac{1}{2}\left( \beta_{01} + \beta_{lm} \right)$.

A tapered structure is modeled assuming an acoustically induced LPG composed of $N$ cascaded of uniforms LPGs with different fiber diameters and lengths $L_i$, as depicted in **Figure 1**.

In each section, since both the velocity ($v$) and the amplitude of the flexural wave depend on the fiber radius, the acoustic wavelength ($\Lambda$) and propagation constant ($\beta$) will have to be computed for each section of fiber. The velocity and amplitude of the acoustic are expressed in function of the fiber radius as

$$v = \sqrt{\pi R c_{ext}}\, f, \tag{9}$$

$$u_0(R) = \frac{R_0}{R} u_0(R_0), \tag{10}$$

where $R_0$ is the original radius of the fiber previous to tapering and where we have assumed that the acoustic power remains constant along the fiber.
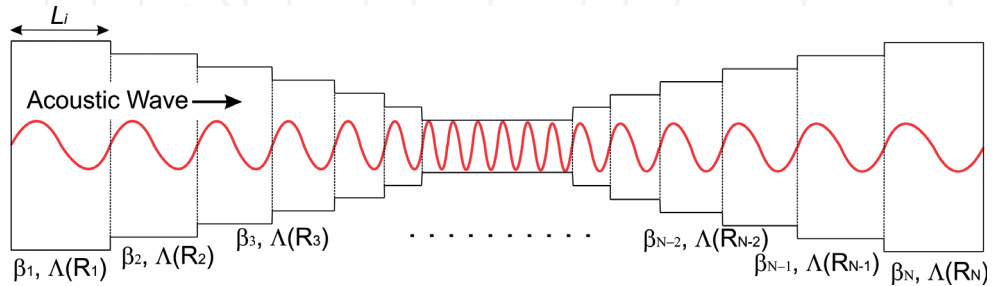


**Figure 1.** Simulation model for the tapered fiber structure.

The output from the $i$th section becomes the input to the $(i + 1)$th section of the fiber. The output from the $N$th section is therefore given by

$$\begin{bmatrix} A(L) \\ B(L) \end{bmatrix} = F_N \cdots F_2 F_1 \begin{bmatrix} A(0) \\ B(0) \end{bmatrix}, \tag{11}$$

where $F_i$ is the $F$-matrix for the $i$th section, as defined by Eq. (8) with $z = L_i$, and $L = \Sigma L_i$ is the total length of the composite tapered fiber. The length $L_i$ is chosen small enough to insure convergence of the numerical simulations.

Finally, the transmission response of the tapered AO device is modeled assuming that only the fundamental mode is launched into the fiber, i.e., $E_{01}(0) \neq 0$ and $E_{lm}(0) = 0$. Thus, the spectral dependence of the core mode is obtained computing $|E_{01}(L)|^2/|E_{01}(0)|^2$ for each optical wavelength. Previously, the specific cladding mode involved in the experiment will be identified after the theoretical analysis of the phase matching conditions of different cladding modes at the frequency of the acoustic wave.

# 3. Acousto-optic devices based on flexural waves

In this section we present experimental results on three different types of AO devices based on acoustic flexural waves. The first device is a conventional acousto-optic tunable attenuation filter, whose transmission characteristics are modeled with the previous transfer matrix analysis. Next, the spectral response of the attenuation filter is improved by the use of tapered optical fibers. The results demonstrate, as it will be shown in Section 3.2, that the geometry of the taper transitions can be regarded as an extra degree of freedom for the design of AO devices. A significant improvement in the spectral bandwidth could be achieved by the proper selection of the fiber transition. Finally, and with the objective of expanding the application of the AO tunable attenuation filters (AOTAF) to an amplitude modulator, acoustic reflection was intentionally induced. Thus, a standing acoustic wave is generated which produces an amplitude modulation at twice the acoustic frequency. Our approach permits the implementation of broad modulation bandwidth (40 nm), high modulation depth (60%), and low optical loss (1.3 dB) in a 70-μm configuration, operating in the MHz frequency range. These experimental results are within the best results reported in the framework of in-fiber AO modulators.

## 3.1. The acousto-optic tunable attenuation filter

A schematic view of the experimental setup to investigate the acousto-optic interaction in optical fibers is depicted in **Figure 2**. The AO device consists of a radio frequency (RF) source, a piezoelectric disk (PD), an aluminum concentrator horn, and an uncoated optical fiber. The PD is excited by the RF source with a sinusoidal waveform to produce an acoustic wave that is transmitted into the fiber through the aluminum horn. To prevent attenuation of the acoustic wave, the fiber is stripped of the outer polymer jacket; and to avoid unwanted acoustic reflections, the acoustic wave is damped at both ends of the uncoated fiber. The length ($L$) of the uncoated optical fiber was selected to be 24 cm. At this length, it is relatively easy to obtain
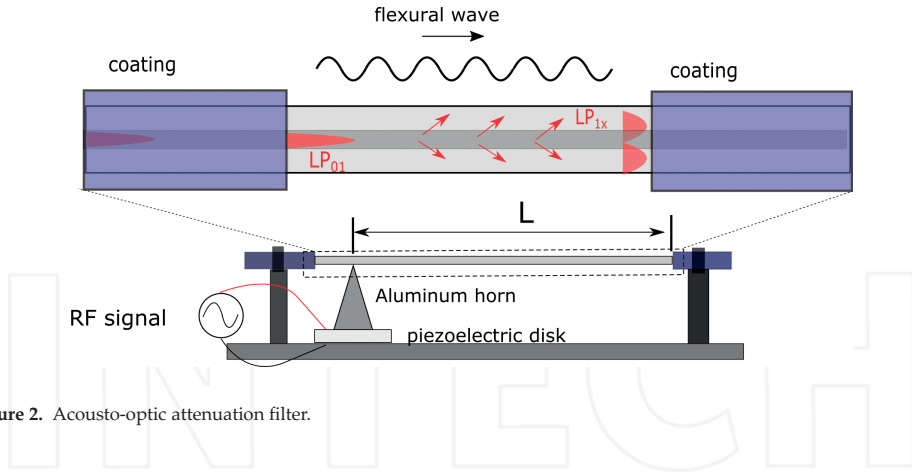
**Figure 2.** Acousto-optic attenuation filter.

a maximum transfer of energy between the core mode and some specific cladding mode of the fiber. Commercially available corning LEAF fiber was used in the experiments to implement AO devices.

Initial experiments were prepared to obtain the flexural wave frequencies that satisfy phase-matching condition between the $LP_{01}$ mode and some specific higher-order cladding mode $LP_{1m}$. The objective is to identify the AO resonances in the experiments to ensure good agreement between numerical simulations and the observed AO interaction. The AO resonances and the spectral response were measured with a superluminescent diode light source (SLD) coupled to the optical fiber that provides an optical spectrum from 1450 to 1650 nm, and the transmission signal is monitored and recorded by an optical spectrum analyzer (OSA). Experimental results of the AO resonances are shown in **Figure 2** for a range of optical wavelengths between 1450 and 1650 nm. Working in the frequency range from 1.6 to 2.8 MHz, $LP_{01}$-$LP_{11}$, $LP_{01}$-$LP_{12}$, and $LP_{01}$-$LP_{13}$ intermodal couplings were observed. The dotted line in **Figure 3(a)** indicates the acoustic frequency of 2.33 MHz, at which three AO resonances were observed with resonant optical wavelengths of 1473, 1537, and 1618 nm, respectively; see **Figure 3(b)**. The voltage applied to the piezoelectric disk ($V_{PD}$) was 33 V (whenever we refer to voltages, it is a peak-to-peak measurement). Beyond this voltage the response of the piezoelectric disk degrades due to an excessive heating. Most of our experiments were carried out using voltages around 30 V, where a stable and linear response of the PD was observed.

The strongest mode coupling was found at the acoustic frequency of 2.005 MHz, corresponding to the $LP_{01}$-$LP_{12}$ intermodal coupling. The spectral dependence of the transmission is shown in **Figure 4**, where experimental (scatter points) and simulation (solid line) results are included. The AO resonance exhibits a maximum rejection efficiency of 15 dB at the optical resonant wavelength of 1596 nm and a 3-dB stopband bandwidth of 1.9 nm. The spectral dependence is calculated using Eq. (8), after computing the modal indexes of the fundamental and high-order cladding modes using a standard boundary-value method, applied to a step index fiber. Material dispersion was estimated assuming a binary silica optical fiber. Experimental results were found
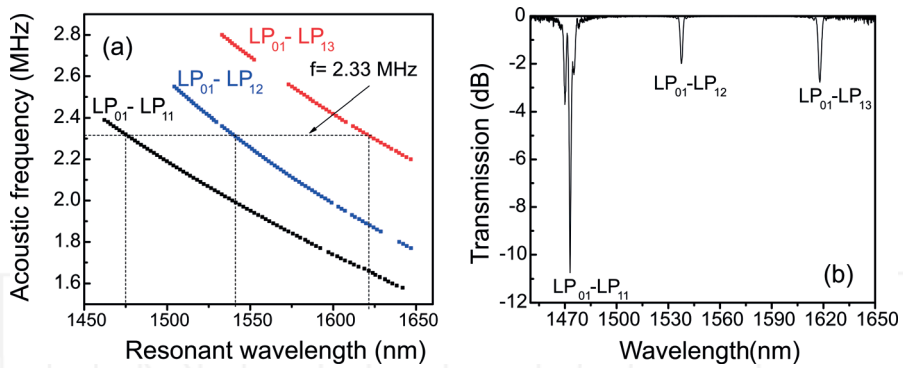
**Figure 3.** Acousto-optic resonances. (a) Acoustic frequency versus resonant optical wavelengths. (b) Transmission response of the AOTAF at the applied frequency of 2.33 MHZ.
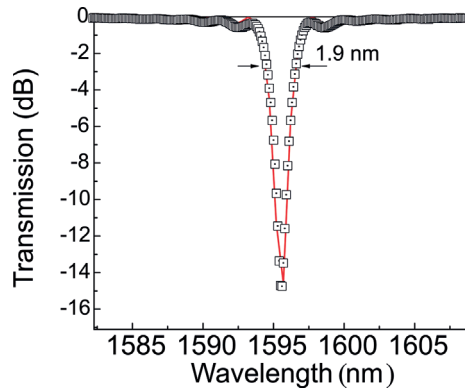


**Figure 4.** Transmittance spectrum at the acoustic frequency of 2.005 Mhz. Scatter points indicate the experimental results, and solid line indicates the simulated transmission.

to be in agreement with simulations by using Sellmeier coefficients for a silica glass doped with $GeO_2$ in the core and pure silica glass in the cladding [17, 18]. Experimental results were best fitted with a $GeO_2$ concentration of around 3.1%, maintaining constant the core radius at 9.3 µm. Simulation parameters were calculated to be closest to the LEAF fiber datasheet.

## 3.2. The acousto-optic tunable attenuation filter with a double-ended tapered fiber

In this section our purpose is to report an improved scheme of AO tunable attenuation filter based on the implementation of thin optical fibers. The proposed configuration combines the advantages of intermodal coupling in a double-ended tapered fiber. The fiber taper was

prepared using a standard fusion and pulling technique, and it was stripped of the outer polymer jacket to prevent the attenuation of the acoustic wave.

In resonance, the resonant wavelength ($\lambda_R$) is directly proportional to the root square of the fiber radius $R$, expressed by the following relation:

$$\lambda_R = (n_{co} - n_{cl}) \sqrt{\frac{\pi C_{ext} R}{f}}, \tag{12}$$

where $n_{co}$ and $n_{cl}$ represent the effective indexes of the fundamental core mode and the cladding mode, respectively. From Eq. (12) it is clear that a small variation in $R$ produces a shift in the resonant wavelength $\lambda_R$. Hence, by imposing a gradual reduction in the fiber diameter, via the tapered fiber, a gradual shift of the resonant wavelength is expected, contributing to enrich the spectral response of the AO device. Furthermore, since the AO effect takes place into a thinner optical fiber, it produces a strong acousto-optic interaction that leads into a more efficient intermodal coupling [19, 20]. Experiments were realized with the same scheme to that shown in **Figure 2** but including a tapered fiber. The fiber was tapered down to a fiber diameter of 80 μm. The length of the tapered fiber is 23.7 cm long, and it was fabricated maintaining relatively long decaying exponential transition profiles. The tapered fiber was composed of 12.5-cm-long uniform taper waist and 5.6-cm-long exponential transitions. **Figure 5** shows the spectral response of the AO interaction. For comparison purposes, and to illustrate the improvement in the spectral response, the transmission spectra for a non-tapered optical fiber are included. In both cases, the acoustic frequency was selected to produce the maximum transfer of energy at a resonant wavelength around 1530 nm. Acoustic frequencies were fixed at 1.23 and 2.49 MHz for the tapered and non-tapered fiber, respectively.
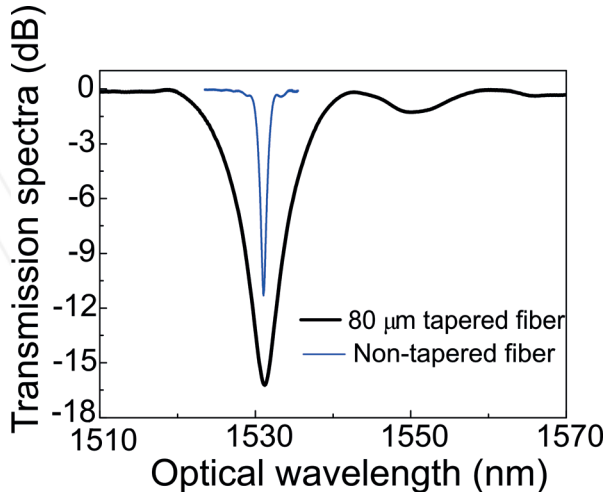


**Figure 5.** Transmission response of an 80-μm tapered fiber (black line). The blue line indicates the transmission response for a non-tapered optical fiber. The acoustic frequencies were fixed to 1.23 and 2.49 MHz, respectively.

The spectral response of the 80-μm tapered fiber exhibits a 3-dB optical bandwidth of 11.68 nm with a minimum transmittance of −16 dB at the resonant optical wavelength of 1531.2 nm. If we compare this result with the spectral response of the non-tapered fiber (12 dB of attenuation and 1.5 nm of optical bandwidth), the improvement achieved by implementing tapered optical fibers is clear.

In order to illustrate how the geometry of the tapered fiber can be used as an extra degree of freedom in the enhancement of the spectral response, we focus our attention on the effects of large tapered transitions as a mechanism to shape the transmission spectrum. The fibers were tapered down to fiber diameters of 80, 70, and 65 μm, respectively. All of them fabricated with long decaying exponential profiles and uniform waists of around ~10 cm in length. The dimensions of the tapered fibers were selected to produce a spectral response that is dependent on the taper transition. **Table 1** shows the parameters of the tapered fibers used in the experiments.

The transmission response of the AO interaction is shown in **Figure 6** for the three tapered fibers. The acoustic frequency was selected to produce a maximum attenuation resonance around 1550 nm, and that corresponded to 0.540, 1.194, and 1.207 MHz for the three tapers of 80, 70, and 65 μm, respectively. The rejection efficiency produced by these tapers was measured as 18, 6.2, and 4 dB, respectively. The red solid line in **Figure 6** indicates the simulated spectral response.

In these experiments, the notch bandwidth undergoes an improved spectral response that is dependent on the fiber diameter. For example, the bandwidth increases from 9 to 45 nm when the waist diameter is reduced from 80 to 70 μm, respectively, and then, the bandwidth reduces to 34 nm for the device with 65-μm waist diameter. This variation in the optical bandwidth can be associated to the spectral contributions of the taper waist and the taper transitions, as it will be

| Waist diameter (μm) | Transition length (cm) | Waist length (cm) |
| --- | --- | --- |
| 80 | 5.06 | 11 |
| 70 | 5.90 | 10 |
| 65 | 5.98 | 9 |

**Table 1.** Parameters of the tapered fibers used in the experiments.
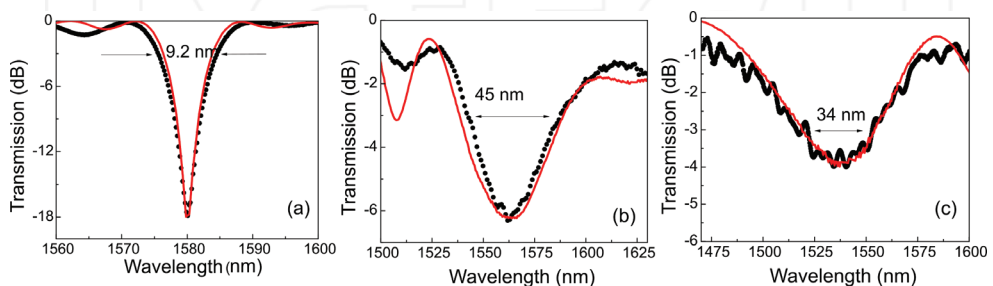


**Figure 6.** Transmission spectra for three different tapered fibers at different acoustic frequencies: (a) 80 μm, (b) 70 μm, and (c) 65 μm waist diameters. In all cases: simulations (solid curve) and experimental values (scatter points). Arrows indicate the spectral bandwidth at −3 dB.

shown below. By comparing these results with a non-tapered single-mode fiber, 1.5 nm of 3-dB optical bandwidth (see **Figure 5**), we observe a 6× to a 30× improvement in the optical bandwidth.

From these results (**Figure 6**) we conclude that our numerical simulations are realistic. Therefore, numeric simulation can be used to gain insight into the AO effect along the tapered optical fiber. For this purpose we have computed the contributions of isolated taper transitions and taper waist. Numerical simulations for the waist and the two taper transitions are shown in **Figure 7** for the three tapered fibers used in the experiments. For the device with 80-μm diameter in **Figure 7(a)**, the greatest contribution comes from the waist region of the device. Then, for the device with 70-μm waist diameter in **Figure 7(b)**, we can observe that the broadening of the notch is enhanced simultaneously by the contribution of both the taper waist and the taper transitions. Finally, for the device with 65-μm waist diameter, **Figure 7(c)**, the role of the taper transitions is the dominant to produce the spectral broadening.

Numerical results demonstrate that tapered transitions can play an important role to improve the optical bandwidth of AO devices. In order to obtain the greatest contribution, the response of taper transitions must be similar to the resonant wavelength of the taper waist. In this way, both elements contribute simultaneously to shape the spectral response of the device. We should also comment that the final transmission of the device is not the simple addition of isolated transmission sections, since a proper concatenation of the taper sections takes into account the amount of power already coupled in the previous sections and the phase accumulated in the each mode.

### 3.3. The acousto-optic amplitude modulator

An important characteristic of the acousto-optic effect occurs when acoustic reflection is induced. Under the effect of a standing flexural wave, the AOTAF can be operated as an amplitude modulator. With the objective of expanding the application of the filter to a broad bandwidth acousto-optic modulator (AOM), we take advantage of the improvements achieved in the spectral response by implementing tapered optical fibers. By firmly clamping one end of the fiber, opposite to the aluminum horn, a standing flexural acoustic wave is generated, and the transmission of the filter can be converted into an amplitude modulation. **Figure 8** illustrates the conversion of the filter into a modulator by the effect of
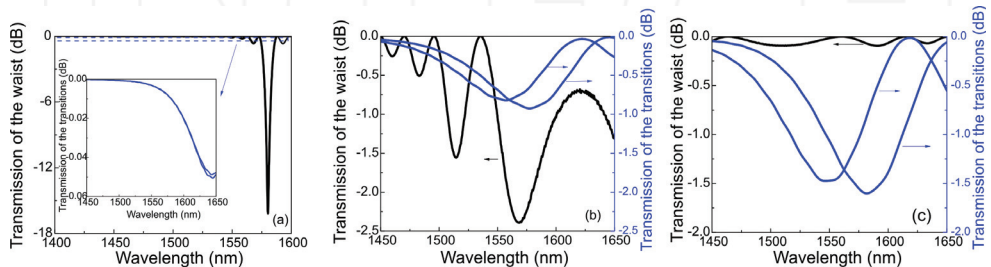


**Figure 7.** Numerical simulations of the spectral response considering the taper transitions and the taper waist as independent parts in the tapered fibers of (a) 80 μm, (b) 70 μm, and (c) 65 μm, respectively.

the standing wave. In this case, the device exhibits a transmission which oscillates in time as a result of the instantaneous perturbation generated by the standing flexural wave. Hence, the transmission is amplitude modulated at a frequency two times the frequency of the acoustic wave.

The AO modulator consists of a 24-cm-long tapered optical fiber, which is composed of two transition sections of 6.38 cm and a uniform waist of 70 μm with 11 cm in length. **Figure 9(a)** shows the spectral dependence including the maximum and minimum transmission for a RF signal applied to the piezoelectric disk of 1.1565 MHz and 10.2 V. From this result we observe a maximum attenuation of 9 dB at the resonant optical wavelength of 1541 nm. At this wavelength the intermodal coupling produces the maximum transfer of energy between the core and cladding modes and consequently the maximum amplitude modulation. The measurements in **Figure 9** were performed with a tunable laser diode (1520–1570 nm) by tuning the wavelength around the resonant wavelength and detecting the transmitted light in a standard oscilloscope. **Figure 9(b)** shows the transmitted light as a function of time at the resonant optical wavelength, for the same conditions described in **Figure 9(a)**. This result demonstrate an amplitude modulation at 2.313 MHz, which is two times the acoustic frequency used in the experiments (1.1565 MHz). The fact that the reflection coefficient for the acoustic wave is not 1 makes the maximum transmission to be slightly below the reference level, i.e., the
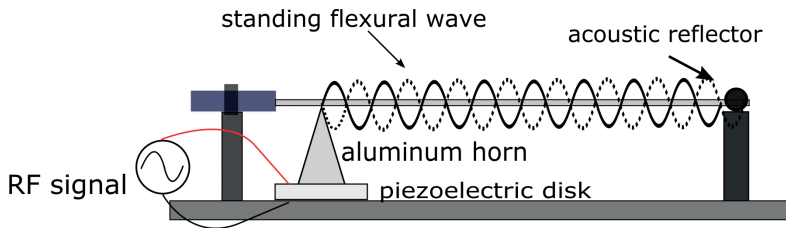


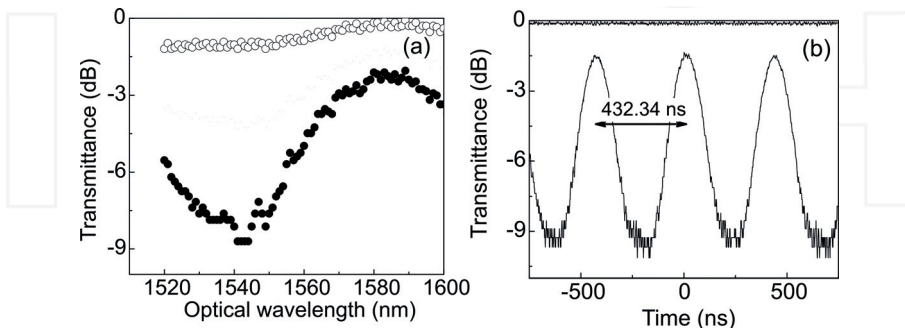**Figure 8.** Acousto-optic amplitude modulator.



**Figure 9.** Transmission response of the AO modulator. (a) Maximum (solid points) and minimum (open points) transmission as a function of wavelength around the resonance located at 1541 nm. (b) Oscilloscope trace of transmitted light at the resonant optical wavelength; the reference level is the 0 dB line. In both cases $f$ = 1.1565 MHz and $V_{PD}$ = 10.2 V.

transmission of the fiber when no acoustic wave propagates. Therefore, the maximum transmission determines the insertion loss of the AOM at a given wavelength, RF frequency, and voltage. The difference between the maximum transmission and the minimum determines the modulation depth. From the results presented in **Figure 9**, we emphasize a strong modulation depth (60.5%), together with a low insertion loss (1.3 dB) and a broad operation bandwidth (~ 40 nm). By comparing the optical bandwidth with a non-tapered AOM [15] (1.5 nm bandwidth), a $26.67\times$ improvement is achieved just by a small amount of reduction in the fiber diameter.

For practical applications, the modulator has a number of specific characteristics that require to be properly analyzed. First, we measured the modulation depth as a function of the optical wavelength, when both the acoustic frequency and the RF voltage were fixed. **Figure 10(a)** shows the modulation dependence around the resonant wavelength of 1541 nm when $f = 1.1565$ MHz and $V_{PD} = 10.2$ V are fixed. At the resonant wavelength, the modulation depth is maximal, and symmetrically decreases for longer and shorter wavelengths. The measured 3-dB bandwidth of the AO modulator is estimated as 40 nm, with a maximum modulation depth of 60.5%. On the other hand, since an acoustic resonator is also formed, **Figure 10(b)** shows the modulation depth versus the detuning frequency $\Delta f$ when $\lambda_R$ and $V_{PD}$ are maintained at 1545 nm and $V_{PD} = 10.2$ V, respectively. The center frequency in **Figure 10(b)** corresponds to 1.1565 MHz. At this frequency the modulation depth is maximal, and it drops gradually to values close to zero around frequencies of $\pm2$ kHz. For longer and shorter frequencies, the transmission oscillates and decays to values near to zero for frequencies around $\pm6$ kHz. Therefore, the proper operation of the AOM is determined by the acoustic frequency $f$, which is selected to achieve the maximum modulation depth.

From a practical point of view, the AOM may find practical applications as active mode locker in all-fiber laser for ultrashort pulse generation. As the results demonstrate, the modulation bandwidth could be as broad as the Erbium band emission (~40 nm), and it could be operated with modulation depths higher that 50%. Beside these benefits, the low insertion losses (< 2 dB) and the inherent advantages of being an all-fiber device should be mentioned. Further improvements in efficiency and interaction length could be possible by properly selecting the geometry of the tapered optical fiber in the modulator.
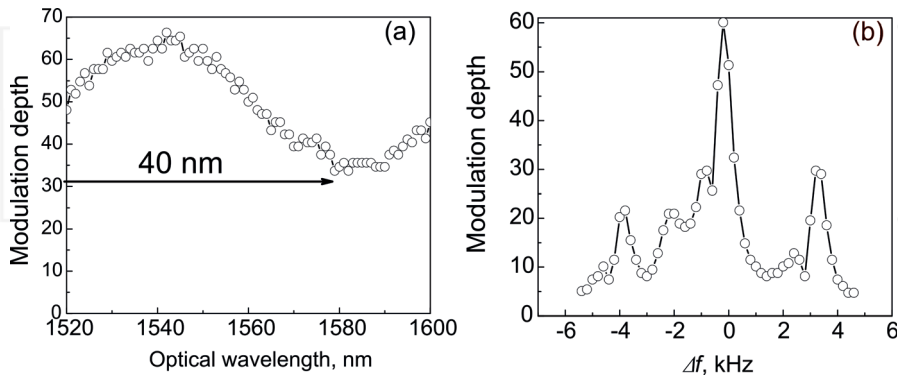


**Figure 10.** Characteristics of the AO modulation. (a) Modulation depth around the resonant wavelength of 1541 nm when $f = 1.1565$ MHz and $V_{PD} = 10.2$ V are fixed. (b) Modulation depth versus the detuning frequency $\Delta f$ when $\lambda_R$ and $V_{PD}$ are maintained at 1541 nm and $V_{PD} = 10.2$ V, respectively. The central acoustic frequency in **(b)** is 1.1565 MHz.

## 4. Conclusions

This chapter demonstrated the potential of in-fiber acousto-optic interaction based on flexural acoustic waves for the design of all-fiber AO devices such as tunable attenuation filters and modulators. Based on the basic theory of AO interaction, the transmission matrix for simulating the acousto-optic response is developed. Numerical results demonstrate good agreement with experimental results. Thus, we can conclude that our numerical simulations are realistic, so we can use the simulation tool to gain insight into the AO interaction along the device. From experimental results, it is demonstrated that the geometry of the taper transitions can be regarded as an extra degree of freedom to the design of AO devices. Optical bandwidths of up to 45 nm are reported in a tapered fiber with a gradual reduction of the fiber. Additionally, under the effect of a standing flexural wave, conventional AO tunable attenuation filters can be operated as an amplitude modulator. As a particular case, an in-fiber AO modulator composed of a double-ended tapered fiber was reported. The fiber taper was prepared using a standard fusion and pulling technique, and it was tapered down to a fiber diameter of 70 μm. The device exhibits an amplitude modulation at 2.313 MHz, which is two times the acoustic frequency used (1.1565 MHz), a maximum modulation depth of 60.5%, 1.3 dB of insertion loss, and 40 nm of modulation bandwidth. From the point of view of implementation, the AOM is well suited for active mode locking in the ultrashort pulse regime.

## Acknowledgements

## Author details

Miguel Ángel Bello Jiménez[1]*, Gustavo Ramírez-Meléndez[1], Erika Hernández-Escobar[1], Andrés Camarillo-Avilés[1], Rosa López-Estopier[1,3], Olivier Pottiez[2], Cristian Cuadrado-Laborde[4], Antonio Díez[5], José L. Cruz[5] and Miguel V. Andrés[5]

*Address all correspondence to: miguel_bello@hotmail.com

1  Research Institute for Optics Communications (IICO), University of San Luis Potosí, San Luis Potosí, S.L.P., México

2  Optics Research Centre (CIO), León, GTO, Mexico

3  National Council on Science and Technology (CONACYT), Mexico, D. F., Mexico

4  Optical Metrology Lab, Institute of Physics Rosario (CONICET-UNR), Rosario, Argentina

5  Department of Applied Physics and Electromagnetism (ICMUV), University of Valencia, Burjassot, Valencia, Spain

## References

[1]  Kim BY, Blake JN, Engan HE, Shaw HJ. All-fiber acousto-optic frequency shifter. Optics Letters. 1986;**11**(6):389-391

[2]  Östling D, Engan HE. Narrow-band acousto-optic tunable filtering in a two-mode fiber. Optics Letters. 1995;**20**(11):1247-1249

[3]  Birks TA, Russell PSJ, Culverhouse DO. The acousto-optic effect in single-mode fiber tapers and couplers. Journal of Lightwave Technology. 1996;**14**(11):2519-2529

[4]  Bello-Jiménez M, Cuadrado-Laborde C, Sáz-Rodríguez D, Díez A, Cruz JL, Andrés MV. Actively mode-locked fiber ring laser by intermodal acousto-optic modulation. Optics Letters. 2010;**35**(22):3781-3783

[5]  Cuadrado-Laborde C, Bello-Jiménez M, Díez A, Cruz JL, Andrés MV. Long-cavity all-fiber ring laser actively mode locked with bandpass acousto-optic modulator. Optics Letters. 2014;**39**(1):68-71

[6]  Alcusa-Sáes EP, Díez A, González-Herráez M, Andrés MV. Time-resolved acousto-optic interaction in single-mode optical fibers: Characterization of axial nonuniformities at the nanometer scale. Optics Letters. 2014;**39**(6):1437-1440

[7]  Culverhouse DO, Richardson DJ, Birks TA, Russell PSJ. All-fiber sliding-frequency Er/Yb soliton laser. Optics Letters. 1995;**20**(23):2381-2383

[8]  Liu WF, Russell PSJ, Dong L. Acousto-optic superlattice modulator using a fiber Bragg grating. Optics Letters. 1997;**22**(19):1515-1517

[9]  Jeon MY, Lee HK, Kim KH, Lee EH, WY O, Kim BY, et al. Harmonically mode-locked fiber laser with acousto-optic modulator in a Sagnac loop and Faraday rotating mirror cavity. Optics Communications. 1998;**149**(4-6):312-316

[10]  Liu WF, Liu IM, Chung LW, Huang DW, Yang CC. Acoustic-induced switching of the reflection wavelength in a fiber Bragg gratting. Optics Letters. 2000;**25**(18):1319-1321

[11]  Zalvidea D, Russo NA, Duchowicz R, Delgado-Pinar M, Díez A, Cruz JL, et al. High-repetition rate acoustic-induced Q-switched all-fiber laser. Optics Communications. 2005;**244**:315-319

[12]  Andrés MV, Cruz JL, Díez A, Pérez-Millán P, Delgado-Pinar M. Actively Q-Switched all-fiber lasers. Laser Physics Letters. 2008;**5**(2):93-99

[13]  Cuadrado-Laborde C, Diez A, Delgado-Pinar M, Cruz JL, Andrés MV. Mode locking of an all-fiber laser by acousto-optic superlattice modulation. Optics Letters. 2009;**34**(7):1111-1113

[14]  Cuadrado-Laborde C, Díez A, Andrés MV. Experimental study of an all-fiber actively mode-locked by standing-wave acousto-optic modulation. Applied Physics B. 2010;**99**(1-2):95-99

[15] Bello-Jiménez M, Cuadrado-Laborde C, Diez A, Cruz JL, Andrés MV. Experimental study of an actively mode-locked fiber ring laser based on in-fiber amplitude modulation. Applied Physics B. 2001;**105**(2):269-276

[16] Erdogan T. Fiber gratting spectra. Journal of Lightwave Technology. 1997;**15**(8):1277-1294

[17] Jeong H, Oh K. Theoretical analysis of cladding-mode wave-guide dispersion and its effects on the spectra of long-period fiber grattings. Journal of Lightwave Technology. 2003;**21**(8):1838-1845

[18] Flemming JW. Material dispersion in lightguide glasses. Electronic Letters. 1978;**14**(11): 326-328

[19] Li Q, Liu X, Peng J, Zhou B, Lyons ER, Lee HP. Highly efficient acoustooptic tunable filter based on cladding erched single-mode fiber. IEEE Photonics Technology Letters. 2002;**14**(3): 337-339

[20] Abrishamian F, Nagai S, Sato S, Imai M. Design theory and experiment of acousto-optical tunable filter by use of flexural waves applied to thin optical fiber. Optical and Quantum Electronics. 2008;**40**(9):665-676